Applied Physics A (2019)125:536
https://doi.org/10.1007/s00339-019-2845-9

Applied Physics A
Materials Science & Processing

Computational understanding of electronic properties of graphene/PtS_2 heterostructure under electric field

Chuong V. Nguyen[1] · Huong T. T. Phung[2] · Khang D. Pham[3,4]

Received: 6 March 2019 / Accepted: 25 June 2019

Abstract
Graphene-based two-dimensional van der Waals heterostructures (vdWH) have recently shown a great potential for high-performance nanodevices. Here, we design a novel vdWH, consisting of the graphene and a noble transition metal dichalcogenide PtS_2 monolayer and investigate its electronic properties as well as the effect of electric field. We find that the key intrinsic characteristics of both the graphene and PtS_2 monolayers are well preserved due to the weak vdW interactions. The graphene is found to form an n-type Schottky contact with the PtS_2 monolayer with a small barrier height of 0.11 eV. Moreover, this small barrier height of the G/PtS_2 vdWH is known to be very sensitive to the external electric field. It can be controlled and turned to the Ohmic contact under electric field. These findings could provide significant knowledge for designing novel electronic and optoelectronic devices of such heterostructure.

1 Introduction

Graphene [1] with the desirable properties has discovered and opened a new direction for future nanotechnologies, especially for high-frequency nanoelectronic devices [2, 3]. However, it has certain limits in applications in nanoelectronics due to the semimetal behavior with zero energy gap [4]. For that reason, in parallel with continuing research to overcome the limitations in graphene, scientists are also advocating for two-dimensional (2D) graphene-like materials with the appropriate electronic, and transport properties for high-performance applications [5–7]. Today, 2D transition metal dichalcogenides (TMDs) are gaining great attention with their promising physical and chemical properties for future applications in electronic and optoelectronic devices [8–12]. Currently, the noble Platinum disulfide (PtS_2) TMD material, a new type of TMDC has received growing attention due to its promising properties for future optoelectronic nanodevices [13–15]. Zhao et al. demonstrated that the PtS_2 material is known to be a layer-dependent indirect bandgap semiconductor [13]. Interestingly, the PtS_2 monolayer has a high carrier mobility of about 1000 cm^2/Vs at room temperature of 300 K. This value is still larger than that of the MoS_2 monolayer [16]. Thus, the PtS_2-based optoelectronic nanodevices may have a better performance than the MoS_2-based nanodevices. These interesting promising properties of the PtS_2 materials make it suitable for future high-performance applications.

Another research field has recently emerged, that is the combination of monolayers of different 2D materials to form layered van der Waals heterostructures (vdWHs). Heterostructures have been shown to have many interesting properties, which do not exist in individual monolayers. Based on these new features, the applications of these materials in high-performance electronic and optoelectronic devices can be opened up. The successful hybridizations between graphene and a variety of other 2D semiconductor materials such as G/TMDs [17–21], G/GaSe [22–24], G/phosphorene [25], G/GaS [26], and so on have recently been synthesized and investigated using different methods both experimentally and theoretically. Theoretically, Ma et al. have studied the electronic properties of G/MoS_2 vdW stacking structures in different stacking patterns by density-functional density theory (DFT) [27]. Jin and his group showed that

✉ Khang D. Pham
phamdinhkhang@tdtu.edu.vn

[1] Department of Materials Science and Engineering, Le Quy Don Technical University, Hanoi, Viet Nam

[2] NTT Hi-Tech Institute, Nguyen Tat Thanh University, Ho Chi Minh City, Viet Nam

[3] Laboratory of Applied Physics, Advanced Institute of Materials Science, Ton Duc Thang University, Ho Chi Minh City, Viet Nam

[4] Faculty of Applied Sciences, Ton Duc Thang University, Ho Chi Minh City, Viet Nam

Published online: 22 July 2019

the G/MoS_2 vdWH forms n-type Schottky contact [21]. Both the Schottky barrier and Schottky contact can be adjusted when placed in an electric field. This result demonstrated the potential application of the G/MoS_2 vdW stacking structure in the high-frequency electronic components [17]. In addition, the G/WSe_2 vdWH heterostructure has also been investigated by DFT calculations [19]. They indicated that the interaction between the graphene and the WSe_2 in this structure is the weak vdW interaction. This weak interaction holds the superior properties of the graphene in such vdWH. At the same time, this structure forms the p-type Schottky contact with a barrier height of 0.51 eV. In particular, they have shown that this barrier height can be adjusted when placed in an electric field or strain, resulting in a transition from p-type to n-type Schottky contact. This feature opens up the potential application of the G/WSe_2 vdWH in the fabrication of future Schottky devices.

Based on the extraordinary properties of the graphene and similar materials, it is possible to predict that these materials possess a number of interesting properties that need to be investigated in detail. These above studies show the great potential applications of monolayer 2D materials and their vdW heterostructure in future nanodevices. However, in addition to their apparent properties, there are many interesting properties that need to be researched to put them into practical application. Moreover, to the best of our knowledge, up to now, there is no literature about the electronic properties of the G/PtS_2 vdWH as well as the effects of electric field on their properties. Therefore, in this work, we design the G/PtS_2 vdWH and investigate its electronic properties at the ground state and under electric field.

2 Computational methods

We perform all the calculations on the basis of DFT method within the Quantum Espresso package [28]. The projection augmented wave (PAW) and the Perdew–Burke–Enzerhof (PBE) functional are used to treat the ion-electron and the exchange-correlation energy, respectively [29]. To correctly describe the weak vdW interactions, we adopt a Grimmes' dispersion corrected DFT-D2 [30]. The energy cutoff is fixed at 500 eV. In the Brillouin zone, a $(9 \times 9 \times 1)$ k point is sampled for both the structural relaxation and electronic property calculations. The atomic structure of the vdWH is fully optimized within the force and total energy convergence less than 10^{-3} eV/Å and 10^{-6} eV, respectively. To calculate the charge transfers between graphene and PtS_2 monolayer (ML), we use a Bader's charge analysis [31–34]. A large vacuum layer thickness of 20 Å along the z direction is adopted to eliminate the interaction between two adjacent periodic slabs.

3 Results and discussion

The G/PtS_2 vdWH was built using the supercell, containing of a (3×3) supercell of graphene and a (2×2) supercell of the PtS_2 ML. In addition, it should be noted that the electronic properties of the PtS_2 ML are known to be very sensitive to strains [35]; thus, in this work, we chosen to fix the lattice parameters of the PtS_2 ML and change the lattice parameters of graphene to match with the PtS_2 ML. After composing the G/PtS_2 vdWH, we find that such vdWH has a small lattice mismatch of 2.7 %, which affects insignificantly the electronic characters of the vdWH. The relaxed atomic structure of the G/PtS_2 vdWH is displayed in Fig. 1. After optimizing the geometric structure of the G/PtS_2 vdWH, we obtain the interlayer distance $D = 3.35$ Å between the G and the PtS_2 layers in the vdWH. It is clear that this distance D is still smaller than the sum of the vdW radii of interfacial carbon and sulfur atoms, indicating that the layers are displaced and the atoms are not strictly on top of each other. This results are also consistent with the intermolecular interactions theory and thus demonstrate the weak vdW interactions in such vdWH. To verify it, we further calculate the binding energy per carbon atom in such vdWH as follows: $E_b = [E_{G/PtS_2} - E_G - E_{PtS_2}]/N$, where E_{G/PtS_2}, E_G and E_{PtS_2} are the total energies of the vdWH, graphene and PtS_2 ML, respectively. N is the number of carbon atoms in the calculated supercell of vdWH. Our calculated E_b is −61.13 meV per C atom. Such E_b value has the same magnitude order as compared to other vdWHs based on graphene, for instance, $E_b = 60$ meV per C atom for G/phosphorene [36], $E_b = 54$ meV per C atom for G/WSe_2 [37], but it is still larger than that in G/WS_2 [38] ($E_b = 26.8$ meV per C atom), G/$MoSe_2$ [39] ($E_b = 21$ meV per C atom). It should be noted that the greater the E_b is, the more stable the vdWH becomes. Thus, we can state that the weak vdW interactions are dominated in such G/PtS_2 vdWH. In addition, the negative value of the E_b indicates that the G/PtS_2 vdWH is energetically favorable.

We now turn to investigate the interesting electronic properties, occurring in the G/PtS_2 vdWH that may not hold in the parent materials. For comparison, we first plot the band structures of the isolated graphene and PtS_2 ML, as shown in Fig. 2a, b, respectively. The isolated graphene shows a metallic behavior with a linear dispersion relation at the Dirac K point, whereas the isolated PtS_2 ML implies a semiconducting character with an indirect bandgap of 1.97 eV. The electronic band structure of the G/PtS_2 vdWH is displayed in Fig. 2c. It is interesting that the electronic band structures of both the isolated graphene and PtS_2 ML are well preserved in the G/PtS_2 vdWH. The nature of this preservation in the vdWH is

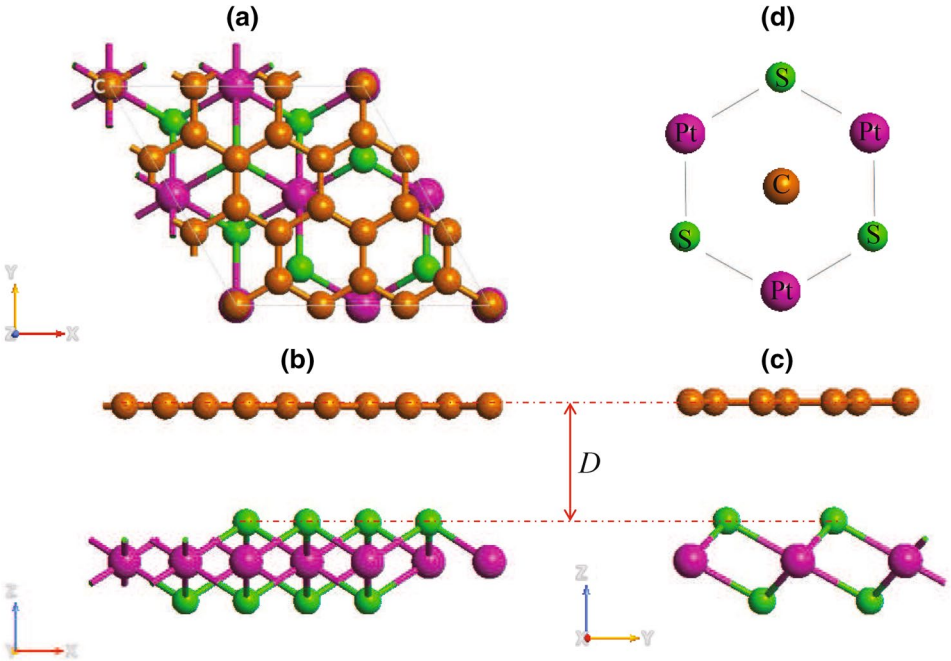

Fig. 1 **a**–**c** Top and side views of the relaxed atomic structure of the G/PtS_2 vdWH. **d** The most stable stacking configuration of the G/PtS_2 vdWH

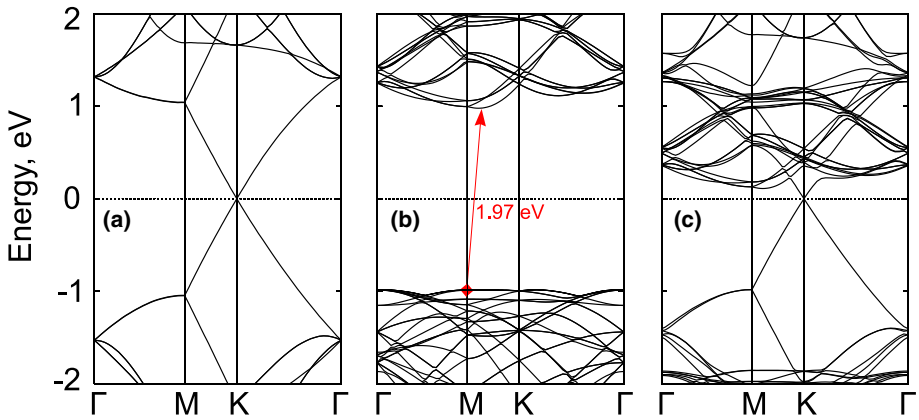

Fig. 2 Electronic band structures of **a** the isolated graphene with a (3 × 3) supercell, **b** PtS_2 ML with a (2 × 2) supercell, and **c** the G/PtS_2 vdWH

due to the weak vdW interactions, which is not enough to modify the electronic properties of both graphene and PtS_2 ML. Thus, the key electronic characteristics of the perfect graphene and PtS_2 ML can be maintained in the G/PtS_2 vdWH. The bandgap of the PtS_2 part in the G/PtS_2 vdWH is almost unchanged as compared with that of the isolated PtS_2 ML. More interestingly, we find that a small bandgap of 8 meV has opened in the graphenes' Dirac cone due to the sublattice symmetry breaking. This observation was also occurred in other vdWHs based on graphene, such as G/MoS_2 [40], G/GaN [41], G/$PtSe_2$ [42, 43], G/GaSe [22] vdWHs, and so on. However, this opened bandgap in the G/PtS_2 vdWH is still smaller than the thermal fluctuations of 26 meV at room temperature; thus, it can be considered negligible and graphene will behave as metallic channel when it placed on the PtS_2 ML to form a metal-semiconductor heterojunction.

We next try to explore in detail the weak vdW interactions in the G/PtS_2 vdWH by establishing the charge transfers between the graphene and PtS_2 layers. Thus, we calculate the charge density difference (CDD) in this vdWH as follows: $\Delta\rho = \rho_{G/PtS_2} - \rho_G - \rho_{PtS_2}$, where ρ_{G/PtS_2}, ρ_G, and ρ_{PtS_2} are, respectively, the charge densities of the vdWH, the isolated graphene, and PtS_2 ML. The CDD in the G/PtS_2 vdWH is displayed in Fig. 3a. One can find that the charges are mostly accumulated in the interfacial area close to the graphene layer, whereas they are depleted mostly in the PtS_2 layer. It also indicates that in the G/PtS_2 vdWH, the charges are directed from the PtS_2 layer to the graphene layer. By Bader charge analyzing, we find that at the equilibrium $D = 3.35$ Å, the charge transference of about 0.082 e electrons are directed from the PtS_2 layer to the graphene layer.

Although the interactions in the G/PtS_2 vdWH are weak and the charger transference from the PtS_2 to the graphene

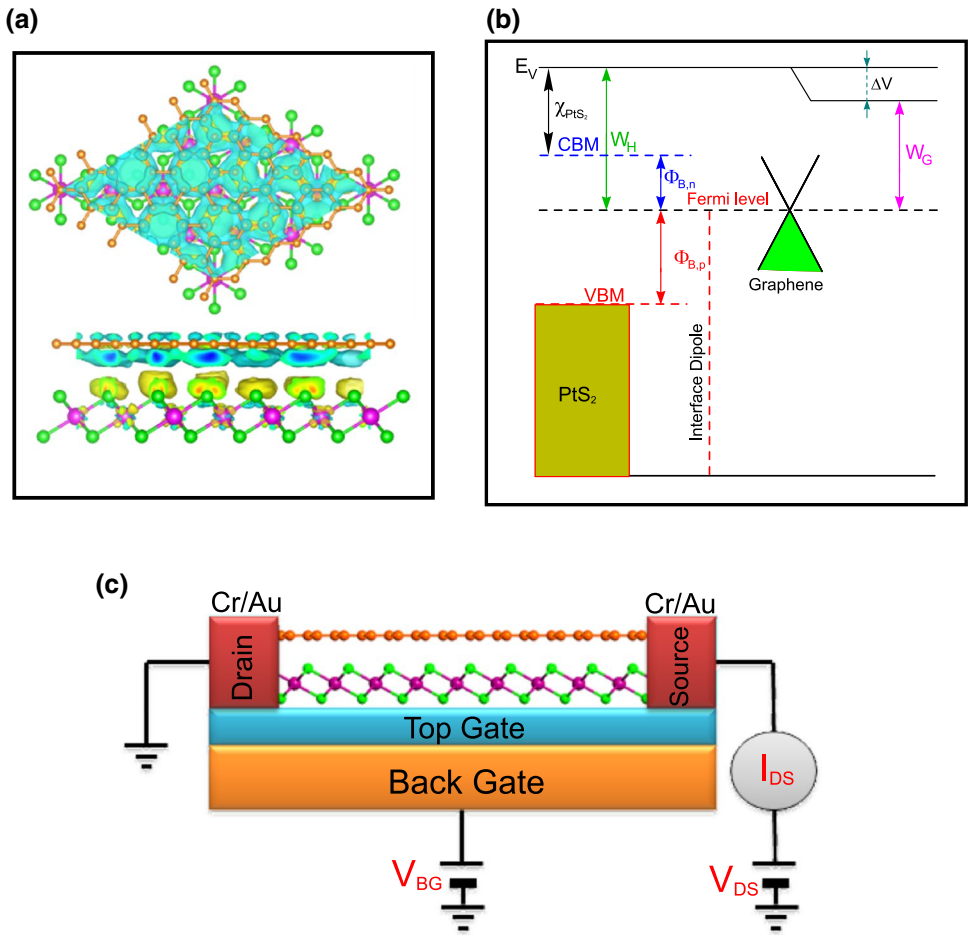

Fig. 3 **a** Charge density difference with an isosurface value of 10^{-3} e/Å^{-3}. The green and yellow areas represent the electron accumulation and depletion, respectively. **b** The energy band diagram of the G/PtS_2 vdWH. **c** The schematic model of FETs based on the G/PtS_2 vdWH

layers is small, it causes an interface dipole that cannot be neglected. This can be connected with a potential step (ΔV) that formed at the heterointerface, as shown in Fig. 3b. The ΔV is the difference in the work functions between the G/PtS_2 vdWH and the graphene, that is $\Delta V = W_{G/PtS_2} - W_G$, where W_{G/PtS_2} and W_G are the work functions of the heterostructure and the isolated graphene, respectively. It should be noted that the G/PtS_2 vdWH represent a metal/semiconductor contact, forming a Schottky or Ohmic contact at the interface. It can be seen from Fig. 3b that the G/PtS_2 vdWH is known to form an n-type Schottky contact at the equilibrium state. The n-type Schottky barrier height of the G/PtS_2 vdWH can be calculated following the Schottky–Mott rule as: $\Phi_{B,n} = W + \Delta V - \chi_{PtS_2}$, where χ_{PtS_2} is the electron affinity of the semiconducting PtS_2 ML. At the equilibrium state, the G/PtS_2 vdWH forms an n-type Schottky contact with a small Schottky barrier height (SBH) of 0.11 eV, which can be easily turned to Ohmic contact.

It is interesting that when G/PtS_2 is used as a component in high-performance nanodevices, it can be subjected to an electric field (E_{perp}), which may cause changes in electronic properties of vdWH. Thus, it is necessary to have a deep knowledge of the effect of the E_{perp} on the electronic properties of such G/PtS_2 vdWH. E_{perp} is applied perpendicular to the heterostructure surface along the z direction, as shown in Fig. 4a. E_{perp}, which pointed from the graphene layer to the PtS_2 layer in the vdWH is defined as the positive direction. As we have mentioned above, the G/PtS_2 vdWH forms the n-type Schottky contact with the $\Phi_{B,n} = 0.11$ eV at $D = 3.53$ Å. It can be seen that when a negative E_{perp} is applied, the $\Phi_{B,n}$ increases, while the $\Phi_{B,p}$ decreases accordingly. Quite the contrary, when a positive E_{perp} is applied to the G/PtS_2 vdWH, $\Phi_{B,p}$ increases, whereas $\Phi_{B,n}$ decreases. These variations are illustrated in Fig. 4b. More interestingly, we find that when a positive $E_{perp} = +1.2$ V/nm is applied, $\Phi_{B,n}$ decreases continuously and reaches zero. It indicates a transformation from the Schottky contact to the Ohmic contact when a positive $E_{\perp} = +1.2$ V/nm is applied to the vdWH.

We now discuss how does the electric field affect the electronic properties of the G/PtS_2 vdWH. The band structures of the G/PtS_2 vdWH under different E_{perp} are plotted in Fig. 5. We find that the Fermi level of the G/PtS_2 vdWH shifts downwards from the conduction band minimum (CBM) to valence band maximum (VBM) of the semiconducting PtS_2 part when a negative E_{perp} is subjected,

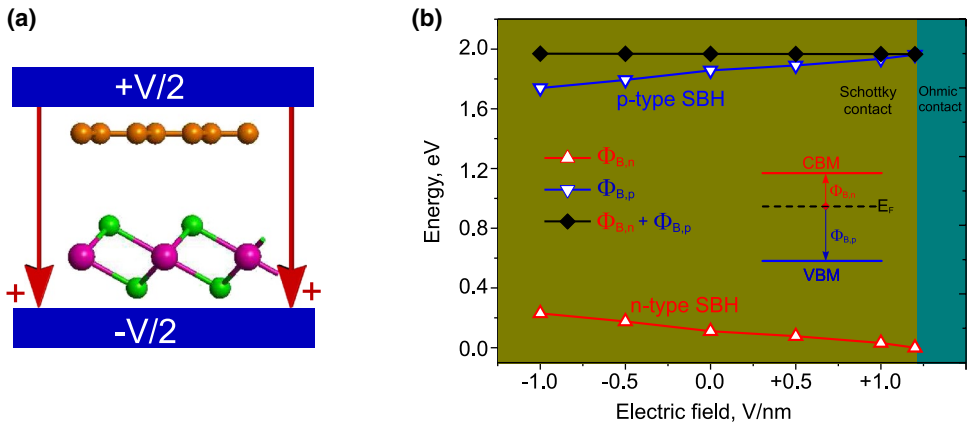

Fig. 4 **a** Schematic model of applied electric field along the z direction of the G/PtS_2 vdWH. **b** Variation of the n-type and p-type Schottky barrier height of the G/PtS_2 vdWH as a function of an applied electric field

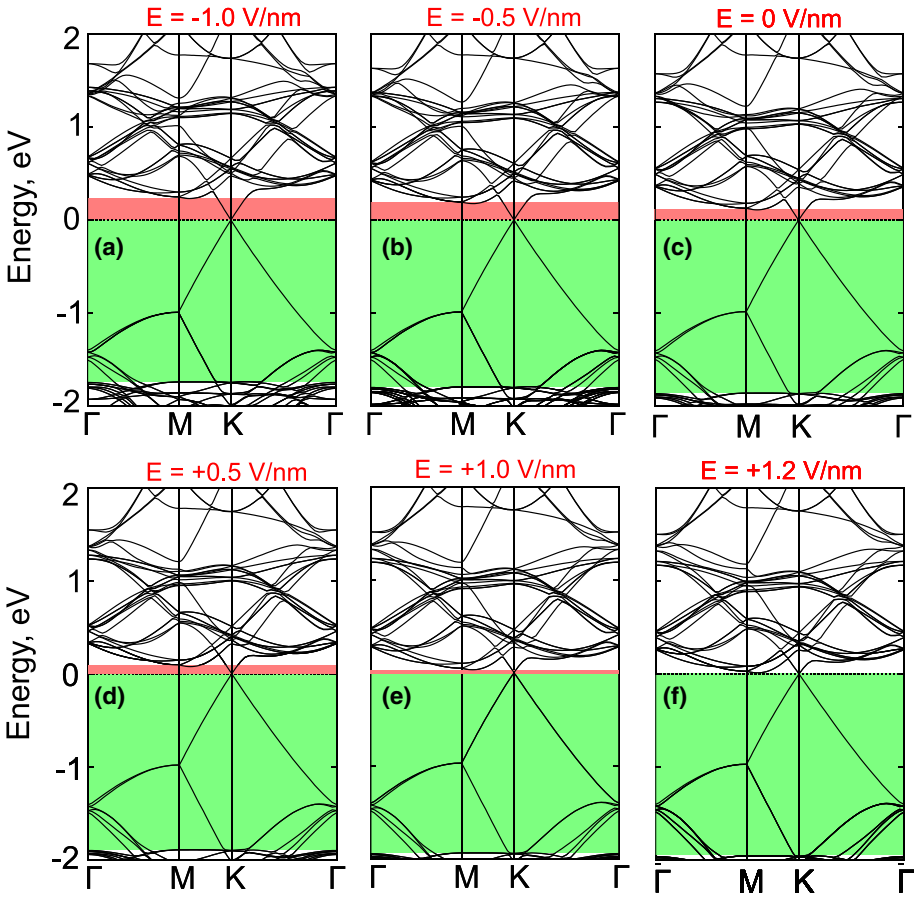

Fig. 5 Electronic band structures of the G/PtS_2 under different $E_{\perp}$ of **a** −1.0 V/nm, **b** −0.5 V/nm, **c** 0 V/nm, **d** +0.5 V/nm, **e** +1.0 V/nm, **f** +1.2 V/nm

as shown in Fig. 5a–c. It leads to a(an) decrease (increase) in the $\boldsymbol{\Phi}_{B,p}(\boldsymbol{\Phi}_{B,n})$, as we have discussed above in Fig. 4b. Quite the contrary, the Fermi level shifts upwards from the VBM to the CBM of the semiconducting PtS_2 part of the G/PtS_2 vdWH when a positive E_{perp} is applied, as shown in Fig. 5d–f. More interestingly, under $E_{perp} = +1.2$ V/nm, the Fermi level shifts continuously and crosses the CBM of the PtS_2 part. Therefore, the n-type Schottky contact of the G/PtS_2 vdWH is turned to the Ohmic contact. The reason of this transformation can be explained as follows. As is well known that in the G/PtS_2 vdWH, the charge transference is pointed from the PtS_2 to the graphene layer, creating a built-in electric field. This built-in E_{perp} leads and the charge transfer in the G/PtS_2 vdWH leads to the change in the position of the Fermi level. When a negative E_{perp} is applied, a built-in E_{perp} and the charge transfer directed from the graphene to the PtS_2 layer. The Fermi level, therefore, shifts downwards from the CBM to the VBM of the PtS_2 part. On

the contrary, when a positive E_{perp} is applied, a built-in E_{perp} and the charge transfer pointed from the PtS_2 to the graphene layer. Thus, the Fermi level moves upwards from the VBM to the CBM of the PtS_2 part, and the n-type Schottky contact are transformed to the Ohmic contact. These findings clearly show that the negative and positive E_{perp} affect differently the band edge positions of the PtS_2 part. This is due to the spontaneous electric polarization, which may originate from the electronegativity difference between carbon and sulfur atoms. Therefore, we can conclude that the Schottky contact of the G/PtS_2 vdWH is known to be strongly sensitive to the E_{perp}, which can turn the n-type Schottky contact to the Ohmic contact. In addition, it should be noted that such a large of electric field, which is required to induce a sizeable effect on the SBH, may be introduced in experiments by gate voltage [44] or by the pulsed ac field technology [45].

4 Conclusion

In summary, we have designed an ultrathin G/PtS_2 vdWH and investigated comprehensively its electronic properties using DFT calculations. We find that in the G/PtS_2 vdWH, the graphene is connected with the PtS_2 layer by the weak vdW interactions with the interlayer spacing of 3.35 Å and the binding energy of −61.13 meV/C atom. It is interesting that the electronic band structures of both the isolated graphene and PtS_2 monolayers are well preserved in the G/PtS_2 vdWH. The nature of this preservation in the vdWH is due to the weak vdW interactions, which is not enough to modify the electronic properties of both graphene and PtS_2 ML. Thus, the key electronic characteristics of the perfect graphene and PtS_2 ML can be maintained in the G/PtS_2 vdWH. The G/PtS_2 vdWH form a p-type Schottky contact with a small Schottky barrier height of 0.11 eV. This small Schottky barrier height of the vdWH can be controlled and turned to the Ohmic contact by applying the electric field. These results provide a valuable information for designing high-performance optoelectronic nanodevices based on the G/PtS_2 vdWH in the near future.

References

1. K.S. Novoselov, A.K. Geim, S.V. Morozov, D. Jiang, Y. Zhang, S.V. Dubonos, I.V. Grigorieva, A.A. Firsov, Science **306**(5696), 666 (2004)
2. F. Schwierz, Nat. Nanotechnol. **5**(7), 487 (2010)
3. L. Vicarelli, M. Vitiello, D. Coquillat, A. Lombardo, A.C. Ferrari, W. Knap, M. Polini, V. Pellegrini, A. Tredicucci, Nat. Mater. **11**(10), 865 (2012)
4. A.C. Neto, F. Guinea, N.M. Peres, K.S. Novoselov, A.K. Geim, Rev. Mod. Phys. **81**(1), 109 (2009)
5. D. Ospina, C. Duque, J. Correa, E.S. Morell, Superlattices Microstruct. **97**, 562 (2016)
6. C.V. Nguyen, N.N. Hieu, C.A. Duque, N.A. Poklonski, V.V. Ilyasov, N.V. Hieu, L. Dinh, Q.K. Quang, L.V. Tung, H.V. Phuc, Opt. Mater. **69**, 328 (2017)
7. A. Tiutiunnyk, C. Duque, F. Caro-Lopera, M. Mora-Ramos, J. Correa, Phys. E **112**, 36 (2019)
8. Q.H. Wang, K. Kalantar-Zadeh, A. Kis, J.N. Coleman, M.S. Strano, Nat. Nanotechnol. **7**(11), 699 (2012)
9. K.F. Mak, J. Shan, Nat. Photonics **10**(4), 216 (2016)
10. D. Jariwala, V.K. Sangwan, L.J. Lauhon, T.J. Marks, M.C. Hersam, ACS Nano **8**(2), 1102 (2014)
11. Q. Tang, Z. Zhou, Z. Chen, Wiley Interdiscip. Rev. Comput. Mol. Sci. **5**(5), 360 (2015)
12. M. Xu, T. Liang, M. Shi, H. Chen, Chem. Rev. **113**(5), 3766 (2013)
13. Y. Zhao, J. Qiao, P. Yu, Z. Hu, Z. Lin, S.P. Lau, Z. Liu, W. Ji, Y. Chai, Adv. Mater. **28**(12), 2399 (2016)
14. L. Li, W. Wang, Y. Chai, H. Li, M. Tian, T. Zhai, Adv. Func. Mater. **27**(27), 1701011 (2017)
15. Y.F. Yuan, Z.T. Zhang, W.K. Wang, Y.H. Zhou, X.L. Chen, C. An, R.R. Zhang, Y. Zhou, C.C. Gu, L. Li, X.J. Li, Z.R. Yang, Chin. Phys. B **27**(6), 066201 (2018)
16. W. Zhang, Z. Huang, W. Zhang, Y. Li, Nano Res. **7**(12), 1731 (2014)
17. D. Pierucci, H. Henck, J. Avila, A. Balan, C.H. Naylor, G. Patriarche, Y.J. Dappe, M.G. Silly, F. Sirotti, A.C. Johnson et al., Nano Lett. **16**(7), 4054 (2016)
18. K. Kim, S. Larentis, B. Fallahazad, K. Lee, J. Xue, D.C. Dillen, C.M. Corbet, E. Tutuc, ACS Nano **9**(4), 4527 (2015)
19. M. Sun, J.P. Chou, J. Yu, W. Tang, J. Mater. Chem. C **5**(39), 10383 (2017)
20. H.C. Diaz, J. Avila, C. Chen, R. Addou, M.C. Asensio, M. Batzill, Nano Lett. **15**(2), 1135 (2015)
21. C. Jin, F.A. Rasmussen, K.S. Thygesen, J. Phys. Chem. C **119**(34), 19928 (2015)
22. Z.B. Aziza, H. Henck, D. Pierucci, M.G. Silly, E. Lhuillier, G. Patriarche, F. Sirotti, M. Eddrief, A. Ouerghi, ACS Nano **10**(10), 9679 (2016)
23. Z.B. Aziza, D. Pierucci, H. Henck, M.G. Silly, C. David, M. Yoon, F. Sirotti, K. Xiao, M. Eddrief, J.C. Girard et al., Phys. Rev. B **96**(3), 035407 (2017)
24. H.V. Phuc, N.N. Hieu, B.D. Hoi, C.V. Nguyen, Phys. Chem. Chem. Phys. **20**(26), 17899 (2018)
25. M. Sun, J.P. Chou, J. Yu, W. Tang, Phys. Chem. Chem. Phys. **19**(26), 17324 (2017)
26. K.D. Pham, N.N. Hieu, H.V. Phuc, I. Fedorov, C. Duque, B. Amin, C.V. Nguyen, Appl. Phys. Lett. **113**(17), 171605 (2018)
27. Y. Ma, Y. Dai, M. Guo, C. Niu, B. Huang, Nanoscale **3**(9), 3883 (2011)
28. P. Giannozzi, S. Baroni, N. Bonini, M. Calandra, R. Car, C. Cavazzoni, D. Ceresoli, G.L. Chiarotti, M. Cococcioni, I. Dabo, A.D. Corso, S. de Gironcoli, S. Fabris, G. Fratesi, R. Gebauer, U. Gerstmann, C. Gougoussis, A. Kokalj, M. Lazzeri, L. Martin-Samos, N. Marzari, F. Mauri, R. Mazzarello, S. Paolini, A. Pasquarello, L. Paulatto, C. Sbraccia, S. Scandolo, G. Sclauzero, A.P. Seitsonen, A. Smogunov, P. Umari, R.M. Wentzcovitch, J. Phys. Condens. Matt. **21**(39), 395502 (2009)
29. J.P. Perdew, K. Burke, M. Ernzerhof, Phys. Rev. Lett. **77**(18), 3865 (1996)
30. S. Grimme, J. Comput. Chem. **27**, 1787 (2006)
31. W. Tang, E. Sanville, G. Henkelman, J. Phys. Condens. Matt. **21**(8), 084204 (2009)
32. E. Sanville, S.D. Kenny, R. Smith, G. Henkelman, J. Comput. Chem. **28**(5), 899 (2007)
33. G. Henkelman, A. Arnaldsson, H. Jónsson, Comput. Mater. Sci. **36**(3), 354 (2006)
34. M. Yu, D.R. Trinkle, J. Chem. Phys. **134**(6), 064111 (2011)

35. G. Liu, Y. Gan, R. Quhe, P. Lu, Chem. Phys. Lett. **709**, 65 (2018)
36. J.E. Padilha, A. Fazzio, A.J.R. da Silva, Phys. Rev. Lett. **114**, 066803 (2015)
37. T. Kaloni, L. Kou, T. Frauenheim, U. Schwingenschlögl, Appl. Phys. Lett. **105**(23), 233112 (2014)
38. F. Zhang, W. Li, Y. Ma, Y. Tang, X. Dai, RSC Adv. **7**(47), 29350 (2017)
39. Y. Ma, Y. Dai, W. Wei, C. Niu, L. Yu, B. Huang, J. Phys. Chem. C **115**(41), 20237 (2011)
40. M. Gmitra, D. Kochan, P. Högl, J. Fabian, Phys. Rev. B **93**(15), 155104 (2016)
41. M. Sun, J.P. Chou, Q. Ren, Y. Zhao, J. Yu, W. Tang, Appl. Phys. Lett. **110**(17), 173105 (2017)
42. S. Sattar, U. Schwingenschlogl, A.C.S. Appl, Mater. Interfaces **9**(18), 15809 (2017)
43. Z. Guan, S. Ni, S. Hu, RSC Adv. **7**(72), 45393 (2017)
44. K.F. Mak, C.H. Lui, J. Shan, T.F. Heinz, Phys. Rev. Lett. **102**(25), 256405 (2009)
45. C. Vicario, B. Monoszlai, C.P. Hauri, Phys. Rev. Lett. **112**(21), 213901 (2014)